Heparan Sulfate Biosynthesis: A Theoretical Study of the Initial Sulfation Step by *N*-Deacetylase/*N*-Sulfotransferase

Anna Gorokhov,*† Lalith Perera,† Thomas A. Darden,* Masahiko Negishi,* Lars C. Pedersen,* and Lee G. Pedersen*†

*National Institute of Environmental Health Sciences, Research Triangle Park, North Carolina 27709 and †Department of Chemistry, University of North Carolina, Chapel Hill, North Carolina 27599-3290 USA

ABSTRACT Heparan sulfate *N*-deacetylase/*N*-sulfotransferase (NDST) catalyzes the deacetylation and sulfation of *N*-acetyl-D-glucosamine residues of heparan sulfate, a key step in its biosynthesis. Recent crystallographic and mutational studies have identified several potentially catalytic residues of the sulfotransferase domain of this enzyme (Kakuta et al., 1999, *J. Biol. Chem.* 274:10673–10676). We have used the x-ray crystal structure of heparan sulfate *N*-sulfotransferase with 3′-phosphoadenosine 5′-phosphate to build a solution model with cofactor 3′-phosphoadenosine 5′-phosphosulfate (PAPS) and a model heparan sulfate ligand bound, and subsequently performed a 2-ns dynamics solution simulation. The simulation results confirm the importance of residues Glu^{642}, Lys^{614}, and Lys^{833}, with the possible involvement of Thr^{617} and Thr^{618}, in binding PAPS. Additionally, Lys^{676} is found in close proximity to the reaction site in our solvated structure. This study illustrates for the first time the possible involvement of water in the catalysis. Three water molecules were found in the binding site, where they are coordinated to PAPS, heparan sulfate, and the catalytic residues.

INTRODUCTION

Biological sulfation, a vital process in living organisms, involves the transfer of a sulfuryl group from the ubiquitous sulfuryl group donor, 3′-phosphoadenosine 5′-phosphosulfate (PAPS), to a wide variety of biomolecules. Sulfation constitutes an integral part of heparin and heparan sulfate biosynthesis. Heparin is synthesized only by mast cells and is more highly sulfated than heparan sulfate, which is produced by most animal cells (Pikas et al., 2000). However, both exhibit a high degree of structural diversity, which is facilitated by the first modification step in the biosynthesis, *N*-deacetylation/*N*-sulfation of D-glucosamine (GlcN) residues. This reaction is catalyzed by a bifunctional Golgi enzyme, *N*-deacetylase/*N*-sulfotransferase (NDST) (Perrimon and Bernfield, 2000). The enzymatic action of NDST predetermines the final structure of the heparan sulfate chains, as the remaining modification steps (epimerization and *O*-sulfation at selected sites) are restricted by the position of the sulfated residues (Pikas et al., 2000). Furthermore, recent studies of the four known isoforms of NDST indicate that each isoform is associated with a specific polysaccharide (NDST-1 is primarily responsible for the sulfation pattern observed in heparan sulfate chains, whereas NDST-2 is associated with heparin synthesis) (Forsberg et al., 1999). Since protein activation, binding, and signaling processes depend on the availability of sulfated glycosaminoglycans, the sulfation mechanism is in effect a prerequisite for the proper functioning of these processes.

In general, sulfated glycosaminoglycans act as universal binding sites for many proteins and growth factors, activating them or helping to localize them on the cell membrane. The list of functions that these sulfated species perform is extensive. Heparan sulfate, for example, plays a role in the coagulation cascade through its enhancement of anticoagulant activity of antithrombin (Berry et al., 1998). It is also involved in cell growth and lipid metabolism (Conrad, 1998). Recently, a novel mechanism of microbial pathogenesis was described that involves sulfated polysaccharides. Certain bacterial species (*Yersinia* and *Staphylococcus*, for example) utilize the ability of heparin and related polysaccharides to serve as binding sites for many other proteins. By recruiting these polysaccharides, bacteria are able to attach themselves to a variety of host proteins without having to develop specific receptors for them (Duensing et al., 1999). Furthermore, sulfated glycosaminoglycans have been implicated in Alzheimer's disease as binding sites for both τ protein and amyloid β peptides, promoting their aggregation in the brain (Bame et al., 1997). Recent genetic studies (Perrimon and Bernfield, 2000) indicate that mutations in NDST homolog in *Drosophila* result in phenotype with severely impaired Wingless (Wg), fibroblast growth factor (FGF), and Hedgehog (Hh) signaling pathways. This study, among with other recent investigations of the Wnt family proteins involved in signaling (Peifer, 1999; Lin and Perrimon, 1999; Payre et al., 1999), demonstrates the importance of NDST for the proper functioning of cellular communication processes.

The ability to understand and control sulfation processes could significantly aid the development of drugs for several medical conditions in which sulfated polysaccharides were found to play a potentially therapeutic role. For example,

Received for publication 30 May 2000 and in final form 12 September 2000.

Address reprint requests to Dr. Lee G. Pedersen, Department of Chemistry, University of North Carolina, Chapel Hill, NC 27599-3290. Tel.: 919-962-1578; Fax: 919-962-2388; E-mail: pedersen@niehs.nih.gov.

0006-3495/00/12/2909/09 $2.00

investigations of tumor growth, HIV, and prion protein diseases such as scrapie report that sulfated polysaccharides act as inhibitors of angiogenesis, virus replication, and prion aggregation, respectively (Parish et al., 1999; Witvrouw and De Clercq, 1997; Caughey and Raymond, 1993). Notably, these studies indicate that the inhibitory activity of these polysaccharides increases with increased molecular weight and degree of sulfation. The mechanisms of sulfation and heparan sulfate biosynthesis, and possible impairment, may therefore be directly connected to the development of disease (Kolset and Salmivirta, 1999).

We have begun our investigation of this complex process with an experimental model based on the x-ray crystal structure of heparan sulfate *N*-sulfotransferase (NST-1) with 3′-phosphoadenosine 5′-phosphate (PAP) bound (Kakuta et al., 1999), as well as the x-ray crystal structures of estrogen sulfotransferase (EST)/PAP/estradiol (Kakuta et al., 1997) and EST/PAP/vanadate complexes (Kakuta et al., 1998). In this study, we explore the solution structure of NST-1. The active site of the enzyme is postulated to be in the open cleft (Kakuta et al., 1999). We find the binding of heparan sulfate precursor (HSP, a GlcA-GlcN disaccharide) to be accompanied by a formation of several hydrogen bonds between the model ligand and residues of this binding site. These interactions help position the HSP in a favorable conformation for an in-line transfer of the sulfate group from PAPS to HSP. Moreover, the sulfuryl transfer mechanism appears to involve several catalytic residues in the PAPS binding site (Lys, Glu, Thr), as well as three or more water molecules. The involvement of water has not previously been discussed as a possible catalytic pathway of sulfotransferases and is a novel feature derived from our study. However, considering the many similarities between sulfuryl and phosphoryl transfer, the involvement of water as a charge-stabilizing species seems reasonable. The proposed mechanism was found to be largely dissociative in character by Bartolotti et al., who studied a greatly simplified reaction model by ab initio and semiempirical quantum mechanical methods (Bartolotti et al., 1999). Here we report a predicted solution structure for the active ternary complex of NST-1, PAPS, and HSP. We find that both associative and dissociative pathways are feasible in our final predicted solution structure, and consequently we must rely on future combined quantum mechanical/classical studies that account for bond breaking/forming to determine which pathway is most favorable (work in progress).

COMPUTATIONAL PROCEDURE

The initial model of the sulfotransferase domain of NDST-1 (residues 580–880) was based on the crystallographic coordinates of NST-1 with PAP bound (pdb entry: 1NST) (Kakuta et al., 1999). The fragments missing from the crystal structure (residues 587–602 and 664–671) were modeled using Sybyl 6.4 loop search (Tripos, St. Louis, MO). Hydrogen atoms were added to the protein, and all crystallographic waters were included in the calculation. Furthermore, the x-ray crystal structure of EST with PAP and vanadate bound (pdb entry: 1bo3) (Kakuta et al., 1998) (specifically, the position of the vanadate with respect to PAP) was used as a guide for modeling the sulfuryl group of PAPS. This was possible because, despite the low sequence homology between NST and EST, the regions important for PAPS binding are conserved between the two enzymes (Fig. 1). PAPS (Fig. 2) was modeled by placing a sulfuryl group in the position occupied by vanadate in the EST crystallographic structure. The geometry of the entire PAPS mole-

```
EST:     1   METSMP----  -EYYEVFGEF  RGVL-----M  DKRFTKYWED  VEMFLARPDD    40
NST :  558   LQTLPPVQLA  QKYFQIFSEE  KDPLWQDPCE  DKRHKDIWSK  -EKTCDRFPK   606

EST:    41   LVIATYPKSG  TTWISEVVYM  IYKEGDVEKC  KEDAIFNRIP  YLECRN----    86
NST :  607   LLIIGPQKTG  TT--ALYLFL  GMHPDLSSNY  PSSETFEEIQ  FFNGHNYHKG   654

EST:    87   ----EDLI--  --NGIKQLKE  KESPRIVKTH  LPPKVLPASF  WEKNCKMIYL   128
NST :  655   IDWYMEFFPI  PSNTTSDFYF  EKSANYFDSE  VAPRRAAALL  --PKAKVLTI   702

EST:   129   CRNAKDVAVS  YYY-------  -FLLMITSYP  NPKSFSEFVE  KF--MQGQVP   168
NST :  703   LINPADRAYS  WYQHQRAHDD  PVALKYTFHE  VITAGSDASS  KLRALQNRCL   752

EST:   169   YGSWYDHVKA  WWEKSKNSRV  LFMFYEDMKE  DIRREVVKLI  EFLERKPSAE   218
NST :  753   VPGWYATHIE  RWLSAYHANQ  ILVLDGKL--  -LPTEPAKVM  DMVQKFLG--   797

EST:   219   LVDRIIQHTS  FQEMKNNPST  NYTMMPEEMM  NQKVSPFMRK  --GIIGDWKN   266
NST :  798   -VTNTIDYHK  TLAFDPKKGF  WCQLLEGGKT  KCLGKSKGRK  YPEMDLDSRA   846

EST:   269   HFPEALRERF  DEHYKQQMKD  C---TVKFRM  EL  295
NST :  847   FLKDYYRDHN  IELSKLLYKM  GQTLPTWLRE  DLQNTR  882
```

FIGURE 1 Alignment of the amino acid sequences of NST and EST. The 5′ PSB loop (residues 613–618 of NST) and the 3′ PB loop (residues 703–715 of NST and additional PAPS-binding residues (833–837, unique to NST)) are shaded. The underlined residues (Lys^{614}, Lys^{676}, Lys^{833}, Glu^{642}, Thr^{617}, Thr^{618}) are most likely catalytic. Adapted from Sueyoshi et al. (1998).

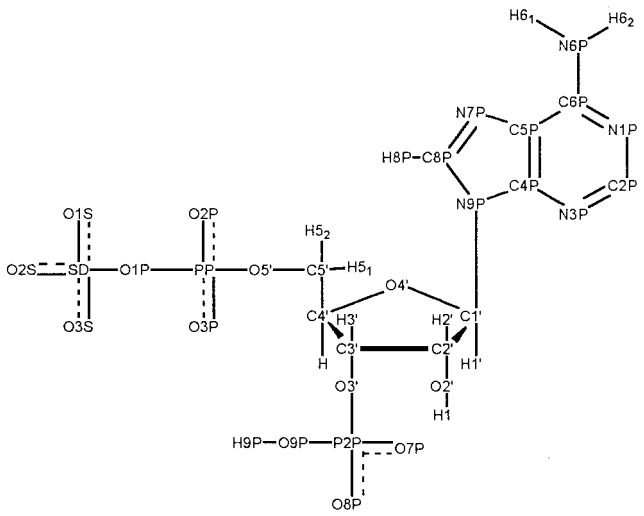

FIGURE 2 3′-Phosphoadenosine 5′- phosphosulfate (PAPS). The −3 anion is shown. The terminal sulfuryl group is not present in the x-ray crystal structure (Kakuta et al., 1999).

TABLE 1 RESP charges for PAPS

PAPS atom	RESP charge	PAPS atom	RESP charge
O1S	−0.7034	C2′	0.0785
SD	1.2546	H2′	0.0692
O2S	−0.7034	O2′	−0.7049
O3S	−0.7034	H1	0.4925
O1P	−0.4419	C1′	−0.0199
PP	1.3157	O4′	−0.3002
O3P	−0.8052	H1′	0.1429
O2P	−0.8052	N9P	−0.0309
O5′	−0.5366	C4P	0.4218
C5′	0.0082	N3P	−0.6178
H51	0.0810	C2P	0.5609
H52	0.0810	H2P	0.0478
C4′	0.0996	N1P	−0.8220
H4′	0.1415	C6P	0.7810
C3′	0.1407	N6P	−0.9977
H3′	0.0776	H61	0.4039
O3′	−0.5204	H52	0.4039
P2P	1.3601	C5P	−0.0123
O7P	−0.8302	N7P	−0.6509
O9P	−0.7498	H8P	0.1252
H9P	0.4417		

The geometry used for charge fitting was obtained with Gaussian98 (3-21 G* basis set) (Frisch et al., 1998). A single point 6-31G* calculation was performed to determine charges based on the optimized geometry.

cule was then energy-optimized by using a 3–21G* basis set of Gaussian 98 (Frisch et al., 1998). After that, a 6–31G* single point calculation was performed based on the 3–21G* geometry, to obtain charges. HSP (Fig. 3) was modeled as a dimer of 1–4 glycosidically linked residues D-glucuronic acid (GlcA) and GlcN, using the Sybyl biopolymer module. The model represents a fragment of a heparan sulfate chain in its initial step of postsynthetic modification, immediately after *N*-deacetylation and before *N*-sulfation. The geometry of this structure was similarly energy-optimized via a 3–21G* basis set of Gaussian 98, and an electrostatic potential grid was obtained with a single point 6–31G* calculation based on the 3–21G* geometry. The charges for PAPS and HSP were fitted using the RESP algorithm (Bayly et al., 1993). These charges are listed in Tables 1 and 2.

Subsequently, the disaccharide was docked into the binding site of NST-1, using Autodock 2.4 (Morris et al., 1996). Grids for computing atom interaction energies were centered on the binding site of the protein. The grid dimensions were 22.5 Å × 22.5 Å × 22.5 Å, and a grid spacing of 0.375 Å was used. The Monte Carlo Simulated Annealing algorithm was applied in two steps. Initially, 25 runs consisting of 50 cycles each were performed. The maximum of accepted or rejected steps for each cycle was set at 100,000. The temperature reduction factor of 0.95 was applied to an initial RT of 616 cal/mol, and the maximum translation step was 0.2 Å. The resulting docked conformations were clustered according to an all-atom RMS deviation, with a cluster tolerance of 0.5 Å. The conformation with the lowest RMS and from the lowest energy cluster was selected and subjected to another 10 docking runs, using the same schedule as in the first docking.

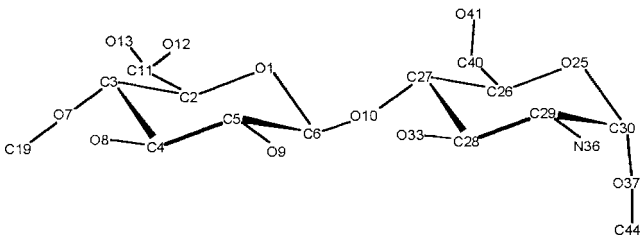

FIGURE 3 Heparan sulfate precursor model. The dimer was created using Sybyl 6.4 (Tripos). It consists of two residues, β-D-glucuronic acid (GlcN) and α-D-glucosamine (GlcA), linked by a 1–4 glycosidic bond. N36 is sulfated by the sulfotransferase.

Three chloride ions were added to counterbalance the total charge of the protein-ligand complex. The system was therefore electrically neutral during the entire simulation.

All energy minimization cycles were accomplished using a combination of conjugate gradient and steepest descent gradient methods. A nonbonded cutoff of 8.0 Å was used (see, however, the more accurate method used for dynamics), with the nonbonded pair list updated at every step.

An energy minimization of the side chains, crystal water hydrogens, and HSP was performed in vacuum for 5000 steps. The system, including crystal water and counterions, was then solvated in a box of 14,493 TIP3P water molecules (Jorgensen et al., 1983). The total number of atoms in the solvated system was 48,447. After solvation, three energy minimization cycles were performed. In the first cycle, the water molecules, HSP, and chloride ions were allowed to

TABLE 2 RESP charges for the HSP

HSP atom	RESP charge	HSP atom	RESP charge
O12	−0.8013	C28	0.3029
C11	0.8211	H35	0.03961
O13	−0.8013	O33	−0.7364
C2	0.1206	H43	0.4788
H14	0.09236	C29	0.1213
C3	0.2509	H38	0.1571
H15	0.05509	N36	−0.4937
O7	−0.4525	H22	0.3476
C19	−0.01628	H42	0.3476
H23	0.07102	H51	0.3476
H24	0.07102	C30	−0.01309
H32	0.07102	H39	0.1633
C4	0.03941	O37	−0.2901
H16	0.06539	C44	−0.1526
O8	−0.7351	H49	0.1146
H20	0.4840	H48	0.1146
C5	0.4053	H50	0.1146
H17	0.03020	O25	−0.3418
O9	−0.7403	C26	0.09856
H21	0.4742	H31	0.1164
C6	0.1938	C40	0.08023
H18	0.1315	H45	0.1259
O1	−0.5349	H46	0.1259
O10	−0.4417	O41	−0.6880
C27	−0.03176	H47	0.4432
H34	0.2560		

The geometry used for charge fitting was obtained with Gaussian98 (3-21 G* basis set) (Frisch et al., 1998). A single point 6-31G* calculation was performed to determine charges based on the optimized geometry.

relax while all other atoms were kept fixed, for 10,000 steps. In the next cycle, the side chains were also allowed to relax in addition to water, HSP, and counterions, for 15,000 steps. Finally, an all-atom energy minimization was performed for 15,000 steps.

A gradual heat-up protocol was then applied to bring the system to 300 K, followed by 25 ps of constant-volume dynamics. All atoms were subsequently reminimized for 15,000 steps. Another gradual heat-up cycle followed at constant pressure. Once the system was heated to 300 K, a constant volume/constant temperature dynamics run was initiated (25 ps). Finally, a constant pressure/constant temperature run was performed for 2 ns. A time step of 1 fs was used for dynamics.

In an initial segment of the simulation (during the 204–214-ps period of dynamics), a constraint was applied to the distance between the nitrogen of the GlcN moiety and the sulfuryl group of PAPS. This constraint was in the form of a harmonic potential and was employed to reduce the distance between N of the GlcN and S of the sulfuryl group from 9 Å to 4 Å in the course of 10 ps. To ascertain that the distance between these two species would naturally reduce to less than 4 Å, a control vacuum dynamics simulation was also initiated for 1 ns. The binding site residues, HSP and PAPS, were allowed to move, while the positions of all other atoms were held fixed. The distance between the HSP and PAPS reduced to 3.8 Å in the course of this simulation.

To observe the effect of bound HSP on the behavior of the enzyme, a second control run in the absence of the ligand was also performed. Finally, an equilibrated structure after 2 ns of dynamics was stripped of all solvent water molecules (excluding the x-ray crystal water), resolvated, and subjected to 300 ps of dynamics, to investigate the behavior of solvent water at the binding site. These three additional dynamics runs were performed following the same protocol for heat-up and equilibration as described above.

All energy minimization and molecular dynamics calculations were performed using Amber, version 5.0 (Case et al., 1999), with the Particle Mesh Ewald method (PME) implemented for calculating long-range interactions (Darden et al., 1993; Essman et al., 1995). Previous studies (York et al., 1993) have indicated the importance of proper treatment of long-range electrostatic interactions for long-time simulations.

RESULTS AND DISCUSSION

Global aspects of the simulation

We carried out a 2.0-ns simulation of NST-1 in the presence of the model HSP disaccharide ligand as well as a 1.0-ns simulation of NST-1 without the ligand. Both structures stabilized in solution. The backbone structure of NST-1 in solution equilibrated within the first 200 ps. The stability of these structures was ascertained by calculating the root mean square deviations (RMSDs) of the backbone atoms, with respect to the x-ray crystal coordinates. An RMSD versus time plot for backbone atoms of NST-1 fluctuates about the value of 1.25 Å for both structures, as shown in Fig. 4. No major disturbances to the tertiary structure resulted from the omission of the ligand. We now present a more detailed analysis of the tertiary complex simulation.

The simulation B-factors ($B_i = 8\pi^2/3\langle\Delta r_i^2\rangle$, where $\langle\Delta r_i^2\rangle$ is the variance in the position of atom i), were calculated for the backbone atoms during the last 500 ps of dynamics (Fig. 5). The x-ray crystal coordinates were used as a reference configuration. The B-factor fluctuation pattern is identical for the backbone atoms N, C, and Cα. Although the general pattern of variance of backbone atoms matches that of the x-ray crystal structure, significant enhancement of some fluctuations is observed upon solvation. The two largest peaks (around residues 587–602 and 664–671) are caused by the fluctuations of those loops that were absent from the crystal structure as they readjust to adopt a favorable configuration in the course of the dynamics. The major thermal fluctuations occur, as expected, at the turn residues or in the random coil. Such is the case for the peaks observed around residues 688–702, 737–741, 758–777, 784–813, and 822–825. An interesting region is found near residues 623–632,

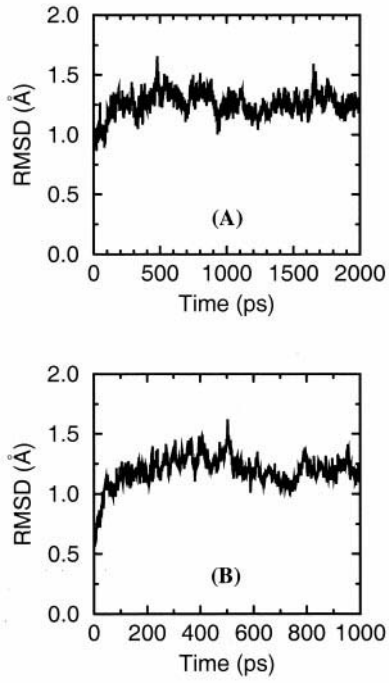

FIGURE 4 Relative mean square deviations (RMSDs) of the backbone atoms. The RMSDs of (*A*) NST with heparan sulfate precursor bound (2-ns simulation) and (*B*) NST without heparan sulfate precursor bound (1-ns simulation) were calculated relative to the positions of the backbone atoms in the x-ray crystal structure (Kakuta et al., 1999).

where the fluctuations occur upon solvation. These fluctuations are most likely due to the loss of crystal contacts in this segment of residues. Moreover, the pattern here can be explained by correlated motion arising from the close contacts of this segment of residues with two highly mobile neighboring loops (residues 587–602 and 664–671).

A plot of α carbon positional deviations with respect to the crystal coordinates (Fig. 6) was obtained to evaluate the changes in the backbone conformation upon solvation. The deviations observed here can be attributed to loss of crystal

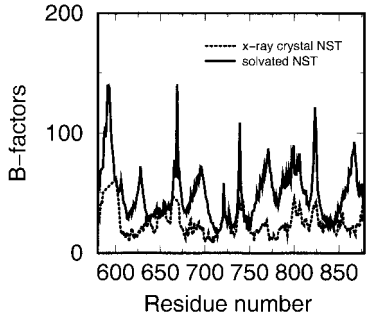

FIGURE 5 B-factors of the solvated NST as compared with the experimental B-factors. The simulation B-factors of the backbone atoms were calculated using the x-ray crystal structure as a reference configuration, over the last 500 ps of the simulation.

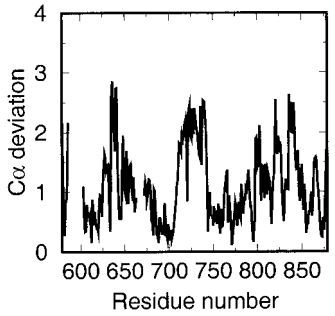

FIGURE 6 Cα deviation for the solution structure of NST. The Cα deviations of the backbone atoms were calculated using the final configuration (after 2 ns of dynamics). The x-ray crystal positions of α carbons were used as a reference. The missing portions of the graph correspond to the residues missing from the x-ray crystal structure.

contacts upon solvation, the rearrangement of residues in the binding loops of PAPS (the 5′ phosphosulfate binding loop (5′PSB loop) and 3′ phosphate binding loop (3′PB loop)) during dynamics, and to the motion of the backbone of external residues under the influence of the solvent. All of these deviations were found to be under 3.0 Å.

Major x-ray crystal contacts that are disrupted upon solvation involve residues 579–586, 601–610, 614, 617, 619, 621,622, 625–629, 631–633, 635, 640, 647, 651, 658, 663, 670–674, 679–701, 704–720, 726–740, 742, 745, 748, 751, 752, 754, 756, 758–773, 775–785, 792, 794–803, 806, 807, 809–852, 854, 855, 866, or 872–877. The important intramolecular contacts observed during the simulation are discussed below.

PAPS binding

The binding of the cofactor PAPS is facilitated by several residues of the 5′-PSB loop (residues 613–618) and the 3′-PB loop (833–837). These residues form an extensive network of hydrogen bonds that anchors PAPS in its binding site.

The hydrogen bonding patterns described in the x-ray crystal structure of NST-1 (Kakuta et al., 1999) are largely preserved in our solvated structure during the course of the simulation (Tables 3, *A* and *B*). In the 5′-PSB loop, the backbone amide nitrogens of Thr^{615}, Thr^{617}, and Thr^{618} form hydrogen bonds with 5′-phosphoryl oxygens of PAPS. Furthermore, the Oγ of Thr^{618} and Thr^{617} are involved in side-chain bonding to the 5′-phosphoryl oxygens. The 5′-PSB segment also contains Lys^{614}. The catalytic importance of this residue has been confirmed by mutagenesis experiments, which demonstrated that the activity of the enzyme was abolished upon K614A mutation (Kakuta et al., 1999; Sueyoshi et al., 1998). Its backbone amide nitrogen as well as the side-chain nitrogen are within hydrogen-bonding distance of the 5′sulfuryl oxygens of PAPS. As the HSP moves into its docked position, an oxygen of the GlcN

TABLE 3 Interactions of binding site residues with PAPS

PAPS	Protein contact	Distance (Å)	Angle (°)
(A)			
O1S	Lys^{614}-N	3.03	154.9
O3S	Lys^{614}-Nξ	2.83	151.6
O2S	Lys^{676}-Nξ	2.82	158.6
O3P	Thr^{615}-N	3.12	153.2
O5′	Thr^{615}-N	2.88	124.8
O3P	Thr^{617}-N	2.97	144.2
O3P	Thr^{617}-Oγ1	2.73	165.0
O2P	Thr^{618}-N	2.81	146.9
O2P	Thr^{618}-Oγ1	2.73	162.5
N6P	Trp^{817}-O	2.95	151.0
O7P	Gly^{834}-N	3.05	162.5
O9P	Gly^{834}-N	3.08	129.8
O9P	Arg^{257}-N	2.95	150.2
(B)			
O1P	Lys^{614}-N	2.91	
O3P	Lys^{614}-Nξ	3.16	
O5′	Gly^{616}-N	3.16	
O2P	Thr^{618}-N	3.15	
O2P	Lys^{833}-Nξ	3.19	
O3P	Lys^{833}-Nξ	3.04	
O9P	Gly^{834}-N	2.95	
O9P	Arg^{835}-N	2.67	
O8P	Ser^{712}-OH	2.51	
O8P	Tyr^{837}-OH	2.65	

(A) 2-ns simulation of NST/PAPS/HSP in solution. The hydrogen bond distances and angles listed in the table are averaged over 20 ps of simulation. The distance and angle cutoff values were 3.2 Å and 110°, respectively. For comparison purposes, the distances between binding site residues and PAP in the x-ray crystal structure are listed in (B).

moiety also forms hydrogen bonds with the side-chain nitrogen of Lys^{614}. It should be noted that during our simulation the Lys residue has shifted from its original position. The contact between the 5′-phosphoryl oxygen and the backbone nitrogen of Lys^{614} observed in the x-ray crystal structure is disrupted in solution, and instead, the nitrogen is bound to an oxygen of the sulfuryl group. Thus Lys^{614} is in a favorable position to neutralize the negative charge of the sulfuryl group.

Additional stabilization of PAPS is provided by the residues of the 3′-PB loop, which mainly form contacts with 3′-phosphoryl oxygens of PAPS. These residues are Gly^{834} and Arg^{835}, which form stable hydrogen bonds with the 3′-phosphoryl oxygens, via the amide nitrogens. Two residues (Ser^{712} and Tyr^{837}) were reported to be within hydrogen-bonding distance in the x-ray crystal structure (Kakuta et al., 1999); however, they move away from PAPS in the course of dynamics. In the case of Ser^{712}, this disruption of the hydrogen-bonding contact is most likely caused by the motion of the helix containing Ser^{712} with respect to its original position. In the case of Tyr^{837}, the side chain is rotated about the Cα-Cβ bond, causing the disruption of the hydrogen bond between the 3′-phosphoryl oxygen of PAPS and Tyr^{837}.

An interesting detail, not possible to observe in the x-ray crystallography study, is the presence of Lys^{676} in close vicinity to PAPS sulfuryl group, in a position where its side chain can form a hydrogen bond with one of the sulfuryl oxygens of PAPS. This side chain also interacts with the side-chain oxygens of Glu^{641} and Glu^{642}.

During the course of the simulation, Lys^{833} is occasionally found in a position to form a hydrogen bond with the 5′-sulfuryl oxygen and so may also serve as a proton donor that neutralizes the negative charge of the sulfuryl group. However, its position is less stable than that of Lys^{614} and Lys^{676}. As in the case of Lys^{614}, the contact of Lys^{833} with the 5′phosphate oxygen is disrupted, because of a motion of this residue toward the sulfuryl group.

Finally, an interaction of Trp^{817} with the N6 nitrogen of the PAPS adenine ring, which was observed in the crystal structure, remained present throughout the simulation. This stabilization of the adenine ring is observed in some nucleotide-binding kinases (Matte et al., 1998) and may be important in positioning the cofactor.

Overall, the important features of the x-ray crystal hydrogen bonding were, for the most part, present throughout the simulation. Contacts with the sulfuryl group oxygens, not present in the x-ray crystal structure, which contained the ligand PAP rather than PAPS, were formed as the three Lys residues (Lys^{614}, Lys^{676}, and Lys^{833}) assumed more favorable positions for neutralizing the negative charge of the sulfuryl group. Similar changes were observed in the dynamics of the protein in the absence of HSP, as well as in the control vacuum simulation, which leads us to conclude that the rearrangements of the Lys positions are not artifacts, but are likely to be of catalytic significance.

Ligand binding

We find that Glu^{641} and His^{716}, as well as three residues of the 5′ and 3′ loops (Gln^{613}, Lys^{614}, and Arg^{835}), form hydrogen bonds with the HSP (Table 4). A bridging water molecule is located between Glu^{642} and the amino group of the GlcN fragment of the HSP. It is possible that Glu^{642} functions as a catalytic base by shuttling a proton via the

TABLE 4 Interactions of binding site residues with the HSP (2-ns simulation of NST/PAPS/HSP in solution)

Heparin atoms	Protein contact	Distance (Å)	Angle (°)
N36	Gln^{613}-Oε1	2.90	119.0
O33	Lys^{614}-Nξ	2.93	119.9
O41	Glu^{641}-Oε1	2.82	146.3
O12	His^{716}-Nε2	2.77	157.1
O12	Arg^{835}-Nη1	2.81	157.0
O13	Arg^{835}-Nη1	2.98	139.3
O13	Arg^{835}-Nη2	2.80	160.4

The hydrogen bond distances and angles listed in the table are averaged over the last 20 ps of simulation. The distance and angle cutoff values were 3.2 Å and 110°, respectively.

bridging water. Several of these residues (Glu^{641}, Glu^{642}, His^{716}) are indicated to be involved, based on recent mutagenesis experiments on NST-1 with a heparan sulfate hexamer (Kakuta et al., unpublished results).

Water involvement in the reaction

The sulfuryl transfer mechanism was first described by Kakuta et al. (1998), based on the investigation of the crystal structure of EST with vanadate ion bound, and mutational analysis. The study identified Lys^{48} of EST as a likely catalytic acid that protonates the phosphate-sulfate bridge oxygen in PAPS, thereby neutralizing the negative charges and stabilizing the dissociation transition state. His^{108} was implicated as a catalytic base that abstracts a proton from the attacking phenol group of the estradiol ligand. Furthermore, Lys^{48}, His^{108}, and Lys^{106} were postulated to stabilize the transition state and enhance the catalytic efficiency of the enzyme. Lys^{48} of EST is conserved in NST-1 (Lys^{614}) and is found in a similar position in the x-ray crystal structure, forming a hydrogen bond with the 5′-phosphoryl oxygen (Sueyoshi et al., 1998; Kakuta et al., 1999). However, we find that upon solvation, Lys^{614} of NST-1 shifts closer to the sulfuryl group. This is not observed in the x-ray crystal structure, most likely because the sulfuryl group is absent. His^{108} is not conserved in NST-1, and its catalytic base function may rather be carried out by Glu^{642}.

We find that several water molecules are present in the binding site during the entire course of the simulation and may be involved in the catalysis. The position of these waters (Fig. 7) was tracked throughout the simulation to determine whether their presence might have any functional significance. Specifically, three water molecules are detected: water 1 is bound to one of the carbonyl oxygens of Glu^{642}, water 2 to the NH_3^+ group of HSP, and water 3 (which is also found in the x-ray crystal structure) to one of the 5′-phosphoryl oxygens. It is important to note that, with the exception of the x-ray crystal water, these sites are occupied by different water molecules at different points in the simulation; i.e., they undergo exchange. Therefore we conclude that, although the waters spend more than the usual residence times in the three sites, they are not simply trapped, but are present to perform a particular function. For example, the water bound to the Glu^{642} of the simulation forms a bridge with a neighboring water molecule, which is in turn bonded to a sulfuryl oxygen of PAPS (this geometry is established during the first 600 ps of dynamics; not shown in Fig. 7). Later in the simulation, these two waters are replaced by a single water molecule (no. 1), which bonds to

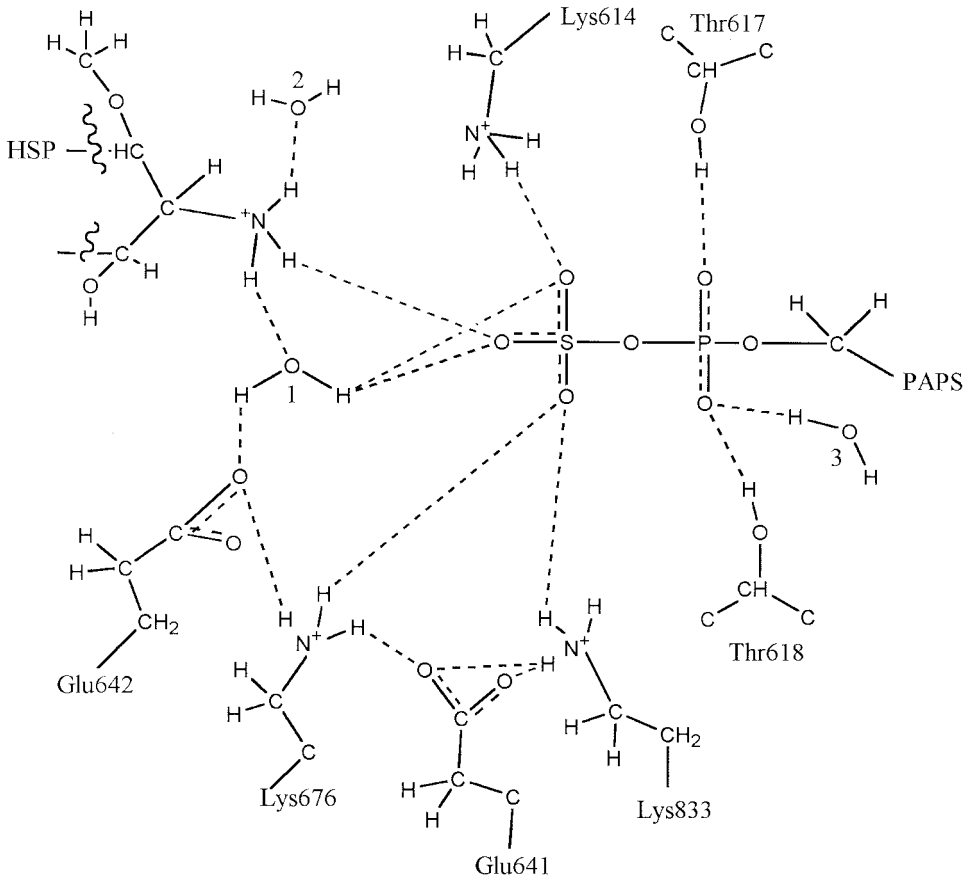

FIGURE 7 Schematic representation of the interactions at the binding site (2-ns simulation of NST/PAPS/heparan sulfate precursor in solution). The hydrogen bonds are represented by the dotted lines. Corresponding hydrogen bond lengths and angles are listed in Tables 3 and 4. The distance between the N of GlcN and the 5′ sulfuryl oxygen is 3.8 Å.

Glu^{642}, GlcN, and PAPS. Based on these observations, we propose that the sulfuryl transfer mechanism may require the participation of water. The water may serve as a proton shuttle between the Glu^{642} and NH_3^+. In this case, Glu^{642} would act as a catalytic base by abstracting a proton from the water, with the resulting hydroxide ion acting to deprotonate the amine group of GlcN. Alternatively, the amine group of GlcN may be deprotonated by water 2, while water 3 provides neutralization for the charges of the 5′-phosphoryl group.

To test this hypothesis, an additional simulation was performed. The NST/PAPS/HSP complex (after a 2-ns simulation) was stripped of all waters and resolvated by the protocol outlined in the Computational Procedure. Subsequently, the system was subjected to a protocol identical to that of the first simulation. The purpose of this control simulation was to ascertain whether water molecules would move to the binding sites where the likely catalytic water molecules were found in the original simulation. After 1 ns of dynamics, two water molecules had migrated to roughly the same locations as waters 1 and 2. One was bound to the nitrogen of GlcN and simultaneously to O3S of PAPS. The second was also bound to the nitrogen of GlcN. The x-ray crystal water (no. 3) remained in its original position, as expected.

Sulfuryl transfer mechanism

Sulfuryl transfer reactions share several key features with the phosphoryl transfer reactions, which have been extensively studied (Mildvan, 1997; Hart et al., 1999). In phosphoryl transfer studies, discussion about whether phosphoryl transfer proceeds via an associative or dissociative mechanism is inevitable. It is reasonable that the various enzyme modes of action favoring associative and/or dissociative transfer are similar in kinases and sulfotransferases. Our solution model provides several possibilities for both associative and dissociative pathways. The key catalytic residues are shown in Fig. 7.

In the case of dissociative sulfuryl transfer, the leaving group (5′-phosphoryl group) gains a negative charge, with the bridging oxygen undergoing the largest change in charge. Therefore, to stabilize the dissociative transition state, the enzyme may provide hydrogen-bonding contacts to stabilize the increasing charge on the 5′-phosphoryl group. The necessary stabilization could be provided by the two Thr residues (Thr^{617} and Thr^{618}) and/or the crystal water molecule that is found in the crystal structure and in the simulation within hydrogen bonding distance of a nonbridging 5′-phosphoryl oxygen (water 3). The proton transfer would not be required in this case, as the hydrogen-bonding interaction of these residues would be sufficient to polarize the charges of the 5′-phosphoryl group.

If one assumes a largely associative mechanism, however, then the largest change in charge occurs on the sulfuryl group being transferred. To stabilize the developing charge on that group, the neighboring residues would likely form a hydrogen-bonding network, with possible proton transfer. In our model, these residues are Lys^{614}, Lys^{676}, Lys^{833}, and a solvent water (water 1). All of these residues are within hydrogen-bonding distance from the sulfuryl group oxygens and could act as proton donors to the transferring sulfuryl group. Their action may be cooperative, as described by Mildvan (1997) for kinases. Therefore, not one but all three residues could be involved in stabilizing the associative transition state. Besides transferring a proton, they also anchor the group in place, positioning it for in-line transfer and reducing the possible degrees of freedom.

The role of the Glu^{642} could be that of a general base, abstracting a proton from a water molecule. This water molecule could be functioning to deprotonate the NH_3^+ group of HSP, to make it a better nucleophile.

In summary, the picture of the reactive site in our simulation presents an extensive hydrogen-bonding network around the 5′ end of PAPS, resulting in several possible paths for the reaction. Some may be more energetically favorable than others, and a combined quantum/classical approach is necessary to decide which path is most energetically favorable (work in progress).

CONCLUSION

We have built a model of NST with PAPS and HSP disaccharide bound, based on the crystal structure of NST with PAP bound, and carried out molecular dynamics simulations on this solvated complex. We find that the structure is stable after 2 ns of dynamics in solution. No large-scale conformational changes were observed. Some local motion of loops occurred during the dynamics, and can be attributed to solvation effects. As expected, the largest motion took place in the loops that were absent from the crystal structure and were modeled in the enzyme, as well as those most exposed to solvent. Some motion of the residues in the binding site in response to the HSP binding was detected.

Our model confirms the importance attributed to the 5′ loop residues, which anchor PAPS and act to stabilize charges on the 5′-phosphoryl and sulfuryl groups. The catalytic residues Lys^{614} and Lys^{833} are in a good position to interact directly with the sulfuryl group being transferred (in addition, our study pointed to a possible involvement of Lys^{676} in catalysis). The Glu^{642} residue may perform the function of a general base. This proposal is confirmed by the fact that Glu^{642} is conserved in several kinases and is associated with a water molecule. A similar water molecule appears in the binding site of several kinases (Wild et al., 1997; Shirakihara and Evans, 1988; Feese et al., 1994) and is likely to play a catalytic role in sulfuryl transfer as well. Two water molecules, in addition to an x-ray crystal water, were found to be important in the sulfuryl binding site; they are possibly involved in deprotonation of the amine group

of the HSP disaccharide, turning it into a better nucleophile. We see several possibilities for the stabilization of either an associative or a dissociative transition state.

We thank Dr. Nancy Thompson at the University of North Carolina (UNC) at Chapel Hill for helpful discussions and critical reading of the manuscript.

This work was supported by the National Institutes of Health (grant HL03650 to LGP) and by the National Institutes of Health (Intramural Research Training Award fellowship to AG). We acknowledge the use of computational resources provided by the North Carolina Supercomputing Center and UNC-Chapel Hill.

REFERENCES

Bame, K. J., J. Danda, A. Hassall, and S. Tumova. 1997. Abeta(1–40) prevents heparanase-catalyzed degradation of heparan sulfate glycosaminoglycans and proteoglycans in vitro. A role for heparan sulfate proteoglycan turnover in Alzheimer's disease. *J. Biol. Chem.* 272: 17005–17011.

Bartolotti, L., Y. Kakuta, L. Pedersen, and M. Negishi. 1999. A quantum mechanical study of the transfer of biological sulfate. *J. Mol. Struct. (Theochem.).* 462:105–111.

Bayly, C. I., P. Cieplak, W. D. Cornell, and P. A. Kollman. 1993. A well-behaved electrostatic potential based method using charge restraints for determining atom-centered charges: the RESP model. *J. Phys. Chem.* 97:10269–10280.

Berry, L., A. Stafford, J. Fredenburgh, H. O'Brodovich, L. Mitchell, J. Weitz, M. Andrew, and A. K. C. Chan. 1998. Investigation of the anticoagulant mechanisms of a covalent antithrombin-heparin complex. *J. Biol. Chem.* 273:34730–34736.

Case, D. A., D. A. Pearlman, J. W. Caldwell, T. E. Cheatham, III, W. S. Ross, C. L. Simmerling, T. A. Darden, K. M. Mertz, R. V. Stanton, A. L. Cheng, J. J. Vincent, M. Crowley, D. M. Ferguson, R. J. Radmer, G. L. Seibel, U. C. Singh, P. K. Weiner, and P. A. Kollman. 1999. AMBER 5. University of California, San Francisco.

Caughey, B., and G. J. Raymond. 1993. Sulfated polyanion inhibition of scrapie-associated PrP accumulation in cultured cells. *J. Virol.* 67: 643–650.

Conrad, H. E. 1998. Heparin-Binding Proteins. Academic Press, San Diego.

Darden, T. A., D. York, and L. G. Pedersen. 1993. Particle mesh Ewald: an N*log(N) method for Ewald sums in large systems. *J. Chem. Phys.* 98:10089–10092.

Duensing, T. D., J. S. Wing, and J. P. M. van Putten. 1999. Sulfated polysaccharide-directed recruitment of mammalian host proteins: a novel strategy in microbial pathogenesis. *Infect. Immun.* 67:4463–4468.

Essman, U., L. Perera, M. L. Berkowitz, T. Darden, H. Lee, and L. G. Pedersen. 1995. A smooth particle mesh Ewald method. *J. Chem. Phys.* 103:8577–8592.

Feese, M., D. W. Pettigrew, N. D. Meadow, S. Roseman, and S. J. Remington. 1994. Cation-promoted association of a regulatory and target protein is controlled by protein phosphorylation. *Proc. Natl. Acad. Sci. USA.* 91:3544–3548.

Forsberg, E., G. Pejler, M. Ringvall, C. Lunderius, B. Tomasini-Johansson, M. Kusche-Gullberg, I. Eriksson, J. Ledin, L. Hellman, and L. Kjellen. 1999. Abnormal mast cells in mice deficient in a heparin-synthesizing enzyme. *Nature.* 400:773–776.

Frisch, M. J., G. W. Trucks, H. B. Schlegel, G. E. Scuseria, M. Robb, J. Cheeseman, V. Zakrzewski, J. Montgomery, R. Stratmann, J. C. Burant, B. Dapprich, J. M. Millam, A. D. Daniels, K. Kudin, M. C. Strain, O. Farkas, J. Tomasi, V. Barone, M. Cossi, R. Cammi, B. Mennuci, C. Pomelli, C. Adamo, S. Clifford, J. Ochterski, G. A. Petersson, P. Y. Ayala, Q. Cui, K. Morokuma, D. K. Malick, A. D. Rabuck, K. Raghavachari, J. B. Foresman, J. Cioslowski, J. V. Ortiz, B. B. Stefanov, G. Lui, A. Liashenko, P. Piskorz, I. Komaromi, R. Gomperts, R. L. Martin, D. J. Fox, T. Keith, M. A. Al-Laham, C. Y. Peng, A. Nanayakkara, C. Gonzalez, M. Challacombe, P. M. W. Gill, B. G. Johnson, W. Chen, M. W. Wong, J. L. Andres, M. Head-Gordon, E. S. Replogle, and J. A. Pople. 1998. Gaussian 98 (Revision A.1). Gaussian, Pittsburgh, PA.

Hart, J. C., D. W. Sheppard, I. H. Hillier, and N. A. Burton. 1999. What is the mechanism of phosphoryl transfer in protein kinases? A hybrid quantum mechanical/molecular mechanical study. *Chem. Commun.* 1:79–80.

Jorgensen, W. L., J. Chandrasekhar, J. D. Madura, R. W. Impey, and M. L. Klein. 1983. Comparison of simple potential functions for simulating liquid water. *J. Chem. Phys.* 79:926–935.

Kakuta, Y., L. G. Pedersen, C. W. Carter, M. Negishi, and L. C. Pedersen. 1997. Crystal structure of estrogen sulphotransferase. *Nature Struct. Biol.* 4:904–908.

Kakuta, Y., Y. Petrotchenko, L. Pedersen, and M. Negishi. 1998. The sulfuryl transfer mechanism. *J. Biol. Chem.* 273:27325–27330.

Kakuta, Y., T. Sueyoshi, M. Negishi, and L. C. Pedersen. 1999. Crystal structure of the sulfotransferase domain of human heparan sulfate N-deacetylase/N-sulfotransferase 1. *J. Biol. Chem.* 274:10673–10676.

Kolset, S. O., and M. Salmivirta. 1999. Cell surface heparan sulfate proteoglycans and lipoprotein metabolism. *Cell. Mol. Life Sci.* 56: 857–870.

Lin, X., and N. Perrimon. 1999. *Dally* cooperates with *Drosophila* Frizzled 2 to transduce Wingless signalling. *Nature.* 400:281–284.

Matte, A., L. W. Tari, and L. T. J. Delbaere. 1998. How do kinases transfer phosphoryl groups? *Structure.* 6:413–419.

Mildvan, A. S. 1997. Mechanisms of signalling and related enzymes. *Proteins.* 29:401–416.

Morris, G. M., D. S. Goodsell, R. Huey, and A. J. Olson. 1996. Distributed automated docking of flexible ligands to proteins: parallel applications of AutoDock 2.4. *J. Comput. Aided Mol. Des.* 10:293–304.

Parish, C. R., C. Freeman, K. J. Brown, D. J. Francis, and W. B. Cowden. 1999. Identification of sulfated oligosaccharide-based inhibitors of tumor growth and metastasis using novel in vitro assays for angiogenesis and heparanase activity. *Cancer Res.* 59:3433–3441.

Payre, F., A. Vincent, and S. Carreno. 1999. ovo/svb integrates Wingless and DER pathways to control epidermis differentiation. *Nature.* 400: 271–275.

Peifer, M. 1999. Signal transduction: neither straight nor narrow. *Nature.* 400:213–215.

Perrimon, N., and M. Bernfield. 2000. Specificities of heparan sulphate proteoglycans in developmental processes. *Nature.* 404:725–728.

Pikas, D. S., I. Eriksson, and L. Kjellen. 2000. Overexpression of different isoforms of glucosaminyl N-deacetylase/N-sulfotransferase results in distinct heparan sulfate n-sulfation patterns. *Biochemistry.* 39: 4552–4558.

Shirakihara, Y., and P. R. Evans. 1988. Crystal structure of the complex of phosphofructokinase from *Escherichia coli* with its reaction products. *J. Mol. Biol.* 204:973–974.

Sueyoshi, T., Y. Kakuta, L. C. Pedersen, F. E. Wall, L. G. Pedersen, and M. Negishi. 1998. A role of Lys614 in the sulfotransferase activity of human heparan sulfate N-deacetylase/N-sulfotransferase. *FEBS Lett.* 433:211–214.

Wild, K., T. Bohner, G. Folkers, and G. E. Schulz. 1997. The structure of thymidine kinase from herpes simplex virus type 1 in complex with substrates and a substrate analogue. *Protein Sci.* 6:2097–2106.

Witvrouw, M., and E. De Clercq. 1997. Sulfated polysaccharides extracted from sea algae as potential antiviral drugs. *Gen. Pharmacol.* 29: 497–511.

York, D., T. Darden, and L. Pedersen. 1993. The effect of long-range electrostatic interactions in simulations of macromolecular crystals—a comparison of the Ewald and truncated list methods. *J. Chem. Phys.* 99:8345–8348.